The role of surface stresses in the deformation of hard elastic polypropylene

C. J. Chou, A. Hiltner and E. Baer
Department of Macromolecular Science, Case Western Reserve University, Cleveland, OH 44106, USA
(Received 25 May 1985)

The phenomenon of stress depression ($\Delta\sigma$) observed when hard elastic polypropylene (HEPP) is exposed to certain liquids has been utilized to probe the role of surface stresses in hard elastic behaviour. Stress depressions were measured in non-interacting liquids and vapours as a function of interfacial surface tension, strain and vapour pressure. Results indicate that surface stress on the microfibres is a significant component of the restoring force. At strains up to 10%, surface stresses from a large number of microfibres contribute about 40% to the restoring force. Above 10% strain, there is no change in the magnitude of the surface contribution. A constitutive equation has been developed from which the fibril diameter can be calculated. Calculated average fibril diameters show that stress-induced subfibrillation is the mechanism responsible for the gradual increase in the surface stress up to 10% strain. Subfibrils are stable only under an imposed stress, the smallest fibril diameter obtained with this material is approximately 20 Å.

(Keywords: hard elastic polypropylene; surface stress; depression; subfibrillation)

INTRODUCTION

In the past two decades, a variety of crystalline and amorphous polymers[1-8] have been processed into what are collectively known as hard elastic materials. These polymers have an interesting combination of mechanical and physical properties including: (1) initial Hookean elasticity, (2) high recoverability from large strains, (3) energetic retractive forces, (4) rehealing after work softening, and (5) constant cross-sectional area during deformation.

Originally, hard elastic polymers were made from crystalline lamellar materials, and were processed via melt spinning and stress crystallization, followed by annealing under tension. The properties of hard elasticity in crystalline polymers have been under intensive investigation by X-ray[9-12], EM[13,14], n.m.r.[15,16], i.r.[17] and other techniques[18-20]. The common structure of these polymers consists of rows of lamellae oriented perpendicularly to the direction of draw. Between these lamellae are microfibrils which are oriented parallel to the draw direction and separated by voids. A typical morphological structure of a hard elastic polymer is shown in *Figure 1*. Many of these materials have been thoroughly reviewed by Sprague[1], as well as Cannon, McKenna and Statton[21].

Over the years, several deformation models were proposed which attempt to relate the mechanical behaviour to the morphology, most of which involved a bending or shearing mechanism of the row structured lamellae. Thus, crystallinity was thought to be an essential criterion for hard elastic behaviour. However, microscopic investigations of deformed hard elastic polyethylene by Miles *et al.*[14] revealed little distortion of the lamellae. In their paper, they also demonstrated an interesting phenomenon of the stress depression of extended hard elastic polyethylene in inert liquid, and concluded that surface tension on the microfibrils was a major contribution to the retractive force. Furthermore, they theorized that the interconnecting microfibrils rather than the lamellae underwent the major deformation.

Several investigators have shown that microfibrils in crazed material can undergo large elastic deformation. Kambour and Kopp[22] first measured the stress–strain behaviour of individual crazes in polycarbonate. They observed that the crazes exhibited rather high elastic recovery. Bucknall *et al.*[23], from the cyclic loading behaviour of high impact polystyrene (HIPS), concluded that the craze fibrils contributed a large portion to the elastic recovery of these deformed materials. It is reasonable therefore that non-crystalline polymers with a fibrillated microstructure may also exhibit hard elastic behaviour. Recently we observed that highly crazed HIPS exhibited the physical and mechanical properties associated with hard elastic crystalline polymers[7,8,24,25] and thus concluded that hard elastic behaviour is due to the bulk-microfibril composite structure independent of crystallinity. Furthermore we suggested that the surface stress on the microfibrils is a substantial component of the restoring force in the hard elastic materials.

The purpose of this work was to study the nature and significance of the surface component of the retractive force in HEPP. This work utilizes the liquid-induced stress depression method to analyse the contribution of surface stress in hard elastic deformation. This stress depression was studied as a function of interfacial surface tension, strain and vapour pressure. The bulk relaxation rate in various media was investigated in order to study the plasticization effect of these media. A model is proposed to explain this unusual phenomenon.

0032-3861/86/030369-08$03.00

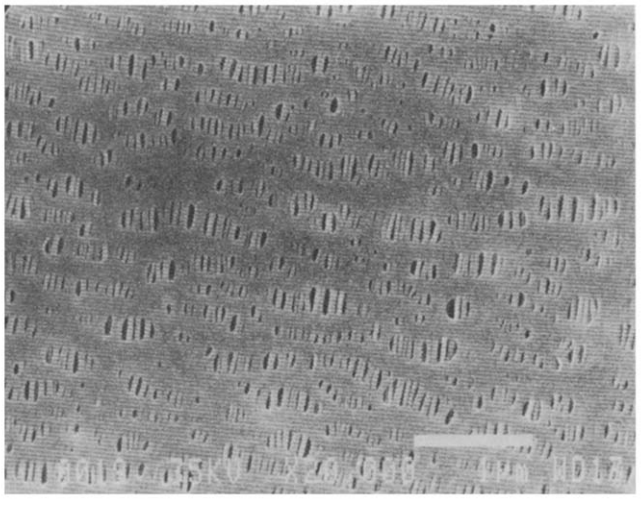

Figure 1 Scanning electron micrograph of Celgard 2400

EXPERIMENTAL

Materials

The materials used in this study were Celgard 2400 and its oriented thin film precursor, generously supplied by the Celanese Corporation. The film, which has a thickness of 25 μ, was cut as received into dumbell-shaped specimens in a direction parallel to the machine direction with a 3 mm width and a 13 mm gauge length. The liquids used were: absolute ethanol from Aaper Alcohol and Chemical Company; deionized water; perfluorinated hydrocarbon liquids from 3M Company; and low viscosity silicone oil from Petrarch Systems, Inc.

Tensile measurements

Tensile measurements were performed using an Instron machine at a strain rate of 4% min^{-1} at room temperature. In stress depression experiments, the materials were stretched to the desired elongation, and the stress was allowed to relax for one hour in order to reach an equilibrium state. The samples were then immersed in a low surface tension, non-swelling liquid. As soon as the liquid, or the vapour of the liquid, made contact with the sample, the equilibrium stress dropped rapidly to a new level which was allowed to stabilize for 10 min. After the removal of the liquid, the stress increased as the liquid evaporated.

Stress depression was also measured in ethanol vapour using a closed system at room temperature. The specimen was stretched to 10% elongation under vacuum. After one hour relaxation, vapour was introduced into the closed system to a given vapour pressure. As in the liquid experiment, the equilibrium stress dropped rapidly to a new level which was allowed to stabilize for 3 min. After the vapour was evacuated from the system, the stress rapidly returned to the original level. After several minutes, fresh vapour was introduced to obtain further data. In one experiment, the vapour pressure was gradually increased from low pressure to the saturation vapour pressure. A second experiment started with the saturation vapour presure and the vapour pressure was decreased stepwise. The results from both experiments were equivalent.

Void volume measurements

To measure void volume in Celgard 2400, samples were stretched to a desired elongation and then immersed in 2 cSt silicone oil. The sample was allowed to imbibe the fluid for 30 min. Excess oil on the sample surface was wiped off before it was unloaded. Upon unloading, the portion of oil forced out of the contracting material was absorbed by preweighed pieces of filter paper. The total mass of oil imbibed in the strained specimens was then determined from the weight of the filter paper and sample. Void volume fraction was calculated by converting the mass of oil into volume and dividing by the volume of the sample.

Contact angle and surface tension measurements

Contact angles between Celgard 2400 precursor film and the various liquids were measured by an NR1 contact angle goniometer (model 100-00, Rame-Hart, Inc., N.J.). Contact angle measurements were made for advancing angles and averages were taken by reading from both sides of each droplet at room temperature. Surface tension of the various liquids was measured by the capillary rise method at room temperature.

RESULTS

Tensile stress–strain behaviour

The cyclic stress–strain behaviour of Celgard 2400 to 60% strain is shown in *Figure 2*. The first cycle shows a gradually decreasing modulus and high recovery upon unloading. On the second cycle, in which the sample is elongated immediately after the first cycle, the initial modulus is lower and the area of the hysteresis loop is

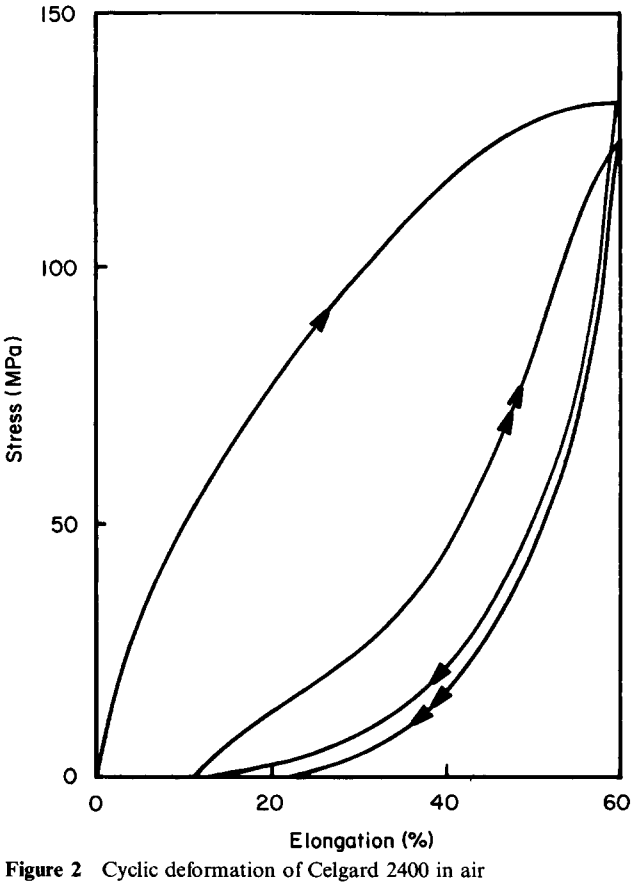

Figure 2 Cyclic deformation of Celgard 2400 in air

much smaller. The third and subsequent cycles are similar to the second cycle.

Void volume

The void volume determined by imbibing silicone oil is shown in *Figure 3*. The material exhibits an initial void volume of about 18% at zero strain which increases to about 65% at 15% strain. There is no further increase in void volume as the material is elongated above 15%.

Liquid-induced stress depression

A typical liquid-induced stress depression experiment is shown in *Figure 4*. The instantaneous stress depression and stress recovery which result from the change in interfacial tension indicate that the surface stress stored on the microfibrils behaves elastically. The stress

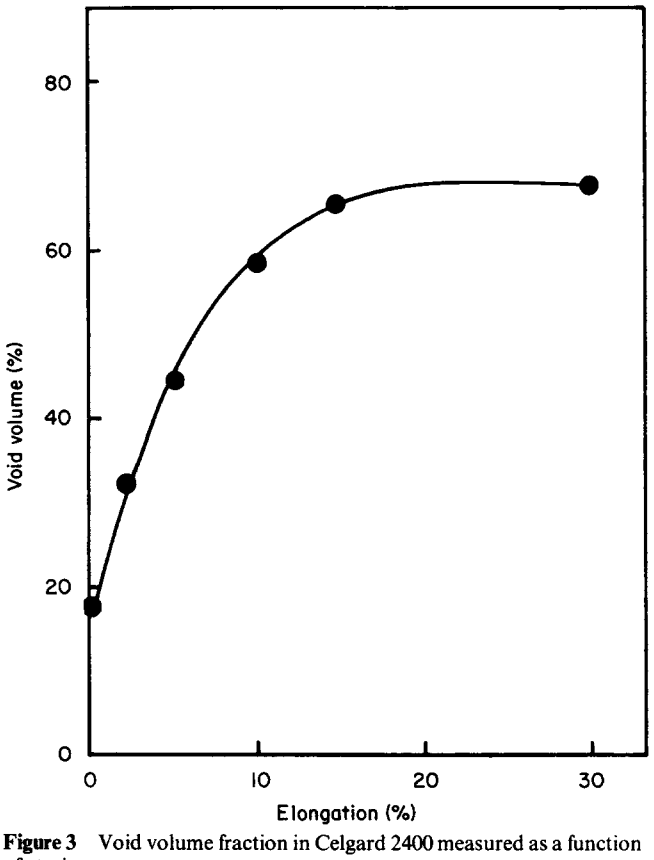

Figure 3 Void volume fraction in Celgard 2400 measured as a function of strain

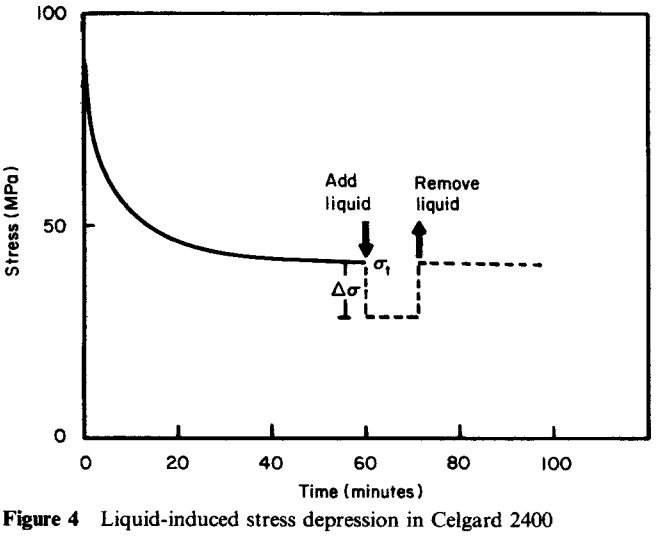

Figure 4 Liquid-induced stress depression in Celgard 2400

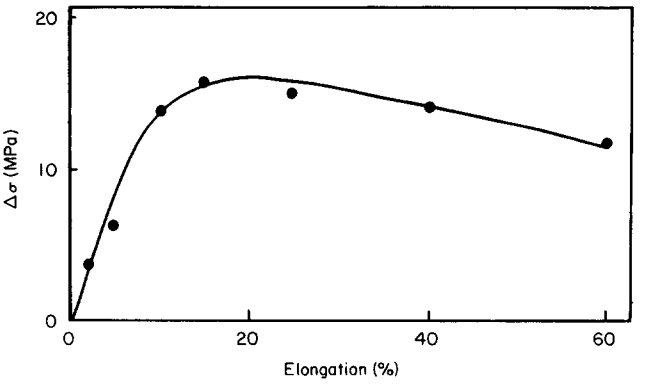

Figure 5 Stress depression of Celgard 2400 as a function of fixed strain

Table 1 Comparisons of stress depressions at the same initial stress level for the first cycle and the second cycle deformation of Celgard 2400 in ethanol

	1st cycle			2nd cycle		
σ_0 (MPa)	$\Delta\sigma$	(σ_t)	$\varepsilon(\%)^a$	$\Delta\sigma$	(σ_t)	$\varepsilon(\%)$
15.7	3.6	(8.9)	(2)	6.2	(9.8)	(22)
29.4	6.2	(15.1)	(5)	9.1	(21.6)	(33)
52.0	13.7	(30.5)	(10)	9.8	(37.9)	(42)
63.7	15.7	(40.2)	(15)	10.4	(45.7)	(45)

[a] See *Figure 4* for definition of σ_0, (σ_t) and $\Delta\sigma$

depression phenomenon was studied in three series of nominally non-interacting liquids. Two of these were found to be unsatisfactory: silicone oil slightly plasticizes Celgard 2400 while perflourinated hydrocarbons with poor wettability[26] did not appear to penetrate the voids. Consequently only the results obtained with ethanol and ethanol/water solutions are reported.

Figure 5 shows the stress depression in ethanol as a function of strain. The magnitude of the effect increases up to 15% strain and then remains essentially constant at higher strains. Correlation between the stress depression results and the void volume measurements clearly indicates that the microfibrillar structure undergoes large changes accompanied by increased surface only during the initial 15% elongation.

When the stress depression was measured on the second loading cycle, after the specimen was strained to 60% as in *Figure 2*, the values were considerably different from these for the first cycle. Numerical values of the stress depression for the first and second cycles are compared in *Table 1* at various stresses. From the large differences, particularly at the lower stresses, it is obvious that the microstructural changes which accompany large deformation are not instantaneously reversible, although with time the specimen will recover most of the original properties[1]. This experiment also shows that the maximum surface effect is obtained at 15% strain on the first cycle, and subsequent cycling does not result in formation of an additional new surface. In fact, the slightly lower stress drop at high deformations on the second cycle suggests that some irreversible damage, such as fibril fracture, may have occurred.

Environmental deformation

The environmental stress depression effect is also observed in the stress–strain behaviour as shown in *Figure 6* where the first cycle in ethanol is compared with

that in air. The instantaneous stress depression was obtained from the difference of the two loading curves (*Figure 7*). The curve is similar to that in *Figure 5*, the stress difference increases with strain up to about 10% elongation and then decreases at higher strains. The maximum stress difference (21.6 MPa) is larger than that

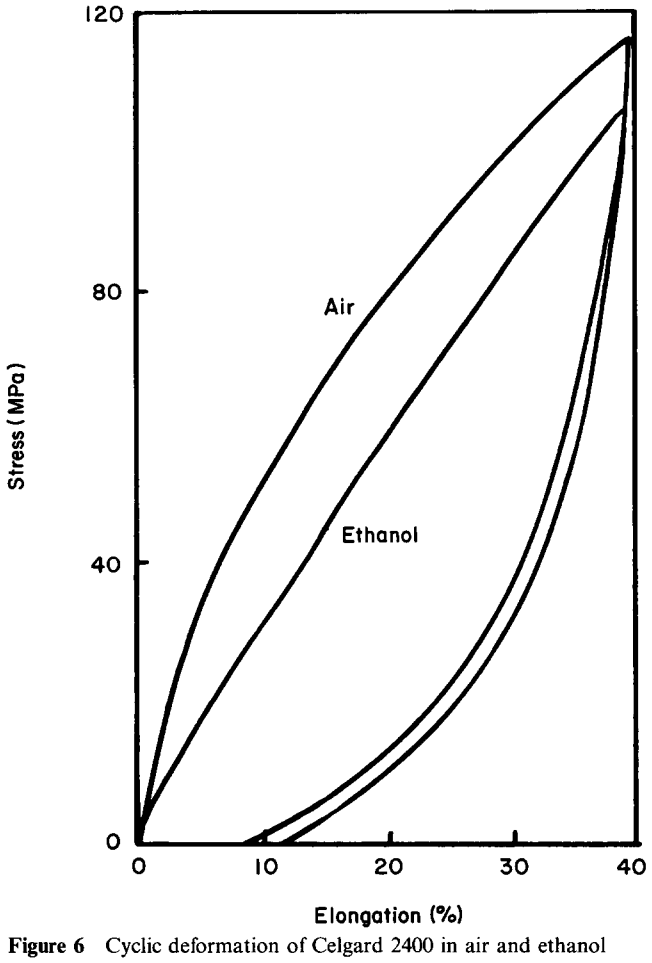

Figure 6 Cyclic deformation of Celgard 2400 in air and ethanol

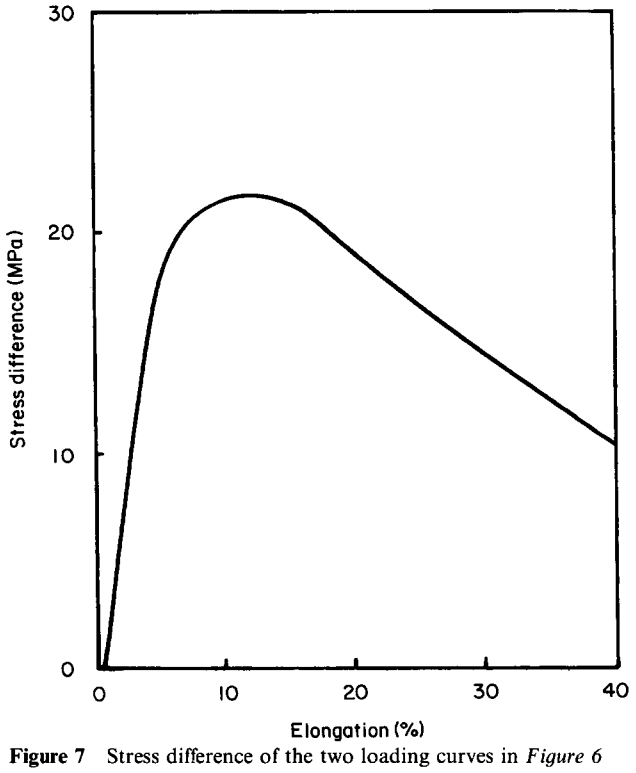

Figure 7 Stress difference of the two loading curves in *Figure 6*

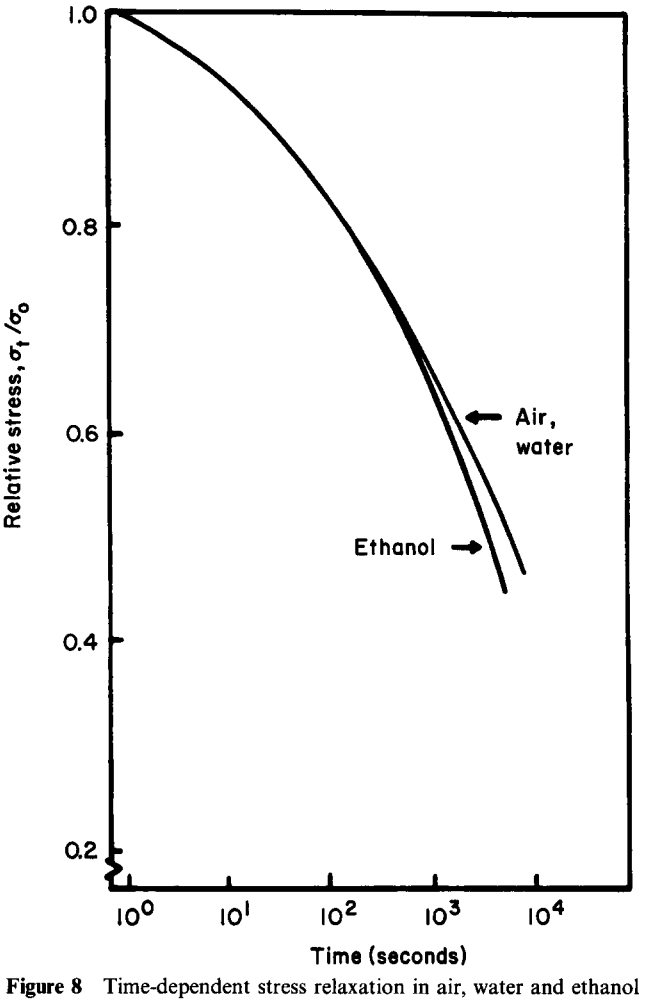

Figure 8 Time-dependent stress relaxation in air, water and ethanol

obtained by the static stress depression method (15.7 MPa). Differences in magnitude between the static and dynamic measurements are manifestations of time-dependent relaxation properties of the material.

Time dependence

The time-dependent stress relaxation in water, ethanol and air over a 3 h period is plotted in *Figure 8*. The bulk relaxation rate should be the same in any non-interacting medium and comparison of the data in *Figure 8* shows that water has no effect on the rate of relaxation over the time period studied. The bulk relaxation rate was also not affected by ethanol for the first 10 min of relaxation, however a slight plasticizing effect is revealed at longer times.

Celgard 2400 shows large time-dependent effects in creep and stress relaxation experiments. The time-dependence of the stress depression in both creep and stress relaxation modes is shown in *Figure 9*. In these experiments, the specimens were allowed to creep or stress relax in air for the indicated time period prior to exposure to ethanol. A different specimen was used for each data point. The time-dependent stress depression was also obtained from the difference between the stress relaxation curves in air and ethanol. The results obtained this way were identical to the stress relaxation results in *Figure 9* except at longer times where small effects of plasticization became apparent. From the results in *Figure 9*, which indicate that the stress depression decreases with time under stress relaxation conditions but is constant in the

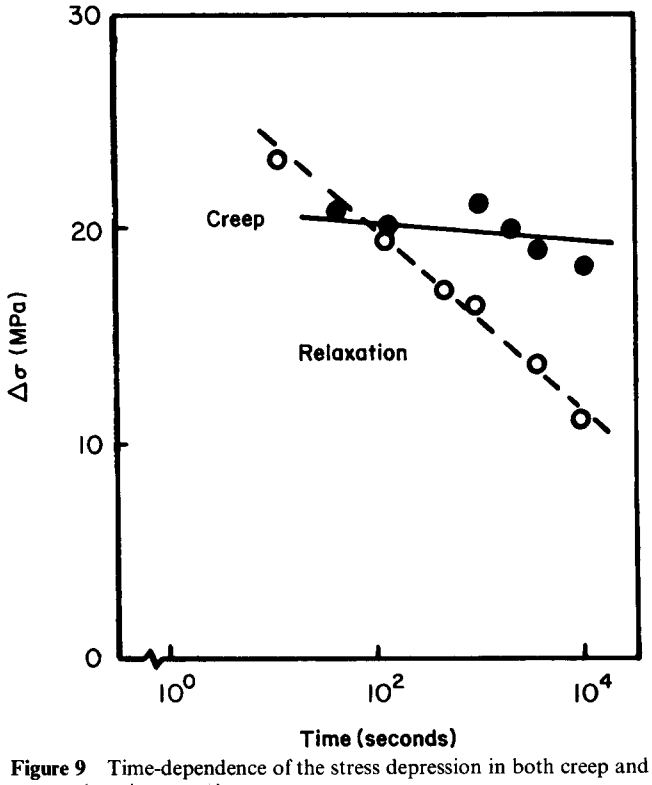

Figure 9 Time-dependence of the stress depression in both creep and stress relaxation experiments

creep experiment, it appears that the surface effect which gives rise to the stress depression is controlled by the applied stress independent of time.

Vapour-induced stress depression

The stress depression phenomenon was also observed in the presence of ethanol vapour. *Figure 10* shows the stress depression relative to that in the liquid as a function of vapour pressure. The shape of the stress depression is similar to the Brunauer type V adsorption isotherm which is specifically observed in the case of multilayer adsorption on porous solids. This suggests that the stress depression phenomenon is purely due to the physical adsorption on the microfibrils surface. The observation of a plateau at high vapour pressure suggests that sorption occurs by capillary condensation. It is not clear why the maximum stress depression achieved in the vapour is only about two thirds of that in the liquid.

Surface tension effects

The relationship between the surface tension of ethanol–water solutions and the stress depression exhibited by Celgard 2400 at 10% strain shown in *Figure 11* is essentially identical to that reported previously[24]. The cricical surface tension of the fibrous material could not be measured directly, but was estimated from contact angle measurements on Celgard 2400 precursor.

Contact angles between Celgard 2400 precursor and the ethanol–water solutions are tabulated in *Table 2* and also plotted by two different methods in *Figure 12*. The critical surface tension of Celgard 2400 precursor estimated from both methods is 20 dynes/cm. This value is much lower than the literature values of 26–29 dynes/cm for polypropylene[27,28], but the high crystallinity and orientation of the precursor material may account for this difference. The surface tension of ethanol is almost equal to the critical surface tension of the precursor. Assuming the critical surface tension of the fibrils is the same as the precursor, surface effects should be eliminated in the experiments carried out in ethanol. Thus, it is possible to attribute 40% of the restoring force at 10% strain to surface stresses on the microfibrils. In addition, the stress–strain curve can be resolved into the bulk and surface

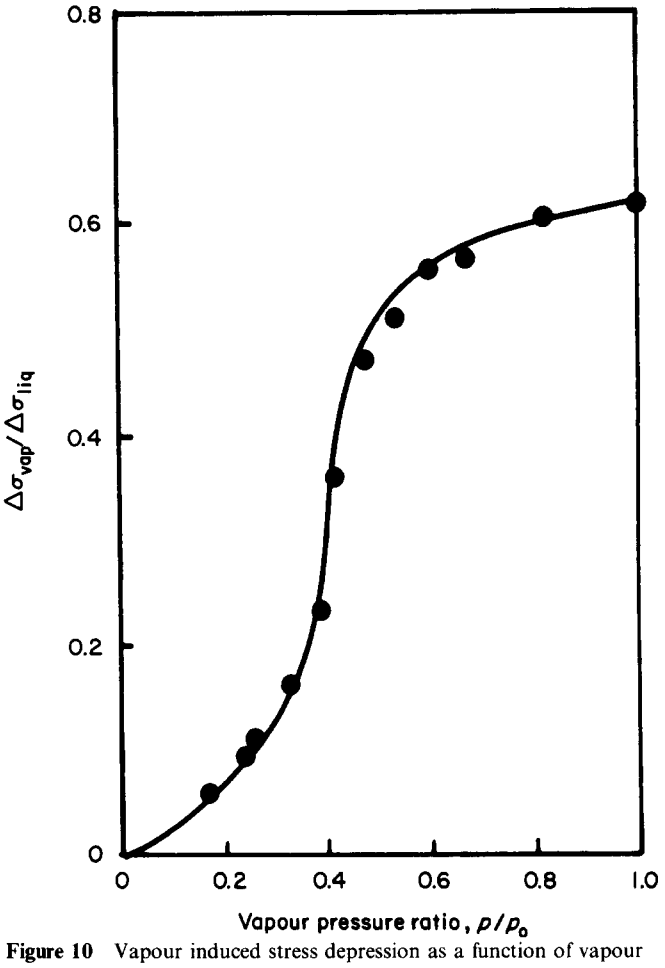

Figure 10 Vapour induced stress depression as a function of vapour pressure

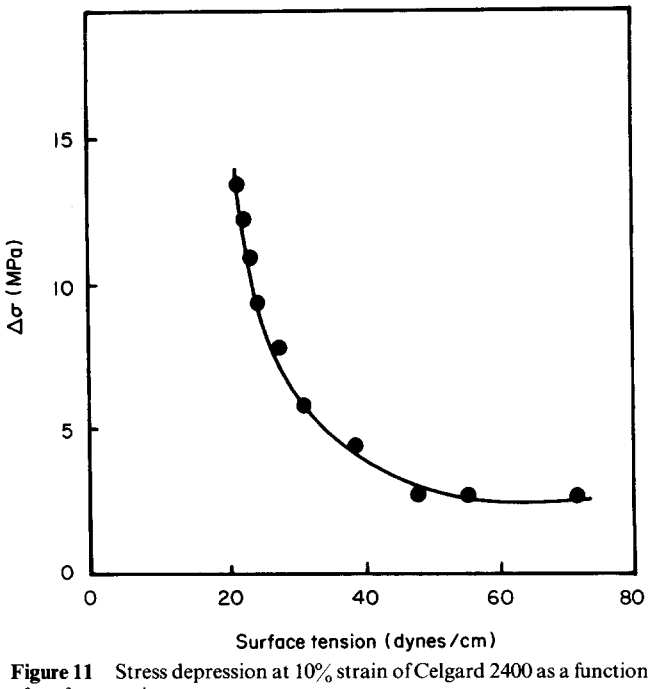

Figure 11 Stress depression at 10% strain of Celgard 2400 as a function of surface tension

Table 2 Calculated average microfibre diameter in Celgard 2400 from experimental contact angles on Celgard 2400 precursor and liquid-induced stress depressions at 10% strain in Celgard 2400 in ethanol–water solutions

Solution (Vol% EtOH)	θ	$\cos\theta$	γ_{LA} (dynes/cm)	$\gamma_{LA}\cos\theta$	$\Delta\sigma$ (MPa)	D (nm)[a]
100	15°	0.97	21.3	20.7	13.7	3.0
95	27°	0.89	22.8	20.3	12.4	3.3
80	38°	0.79	23.7	18.7	11.1	3.4
60	46°	0.69	24.7	17.0	9.5	3.6
48	56°	0.56	27.6	15.6	7.8	4.0
34	66°	0.41	31.1	12.8	5.9	4.3

[a] Calculated by assuming $A_f = 0.5$

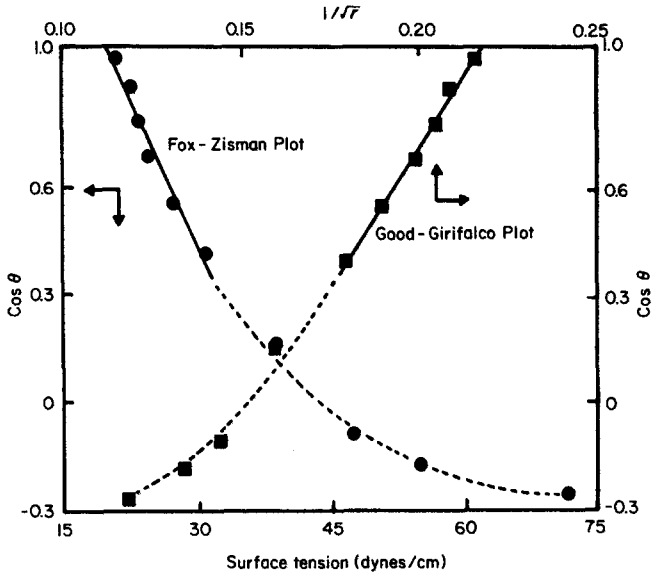

Figure 12 Contact angle data for ethanol–water solutions on Celgard 2400 precursor

contributions. The bulk component is given by the stress–strain curve in ethanol (*Figure 6*), and the difference curve in *Figure 7* is the surface contribution.

DISCUSSION

Constitutive equation under uniaxial tension

The stress-induced subfibrillation mechanism proposed previously for hard elastic materials derives from the common morphological features. Best illustrated by hard elastic polypropylene, this structure consists of parallel rows of lamellae connected by fibrils about 200 Å in diameter. The voids between these fibrils give the material its characteristic high void volume. Under uniaxial tension, it has been suggested that the fibres of relatively small diameter are in a uniaxial stress state and due to Poisson's ratio contract in the perpendicular direction with the result that they split into numerous microfibrils (*Figure 13*). Experimental support for the subfibrillation mechanism in hard elastic materials is provided by the increase in the magnitude of the stress depression. To obtain the relationship between stress depression and microfibril structure, it is recognized that the work to form new surface depends on the surface area, but once formed, the surface component of the restoring force depends on the circumference of the fibril.

For a single cylindrical fibre subjected to uniaxial stretch, the total restoring force on the fibre, denoted by F_T, has an elastic and a surface component. At an

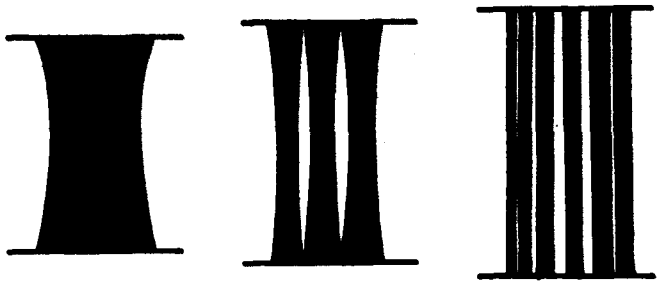

Figure 13 Proposed model of fibril subfibrillation

extension ε, the elastic component is given by

$$F_E = \frac{\pi D^2}{4} E\varepsilon \tag{1}$$

where D is the diameter of the stretched fibre and E is the Young's modulus of the fibre. The surface component of the restoring force is a function of fibre circumference, πD, and interfacial surface tension γ, and is given by

$$F_S = \pi D\gamma \tag{2}$$

Therefore, the total restoring force on the fibre is

$$F_T = F_E + F_S = \frac{\pi D^2}{4} E\varepsilon + \pi D\gamma \tag{3}$$

or the total stress on the fibre is

$$\sigma = \frac{F_T}{A} = E\varepsilon + \frac{4}{D}\gamma \tag{4}$$

where A is cross-sectional area of the fibre.

Specifically, the stress measured in air is

$$\sigma_{SA} = E\varepsilon + \frac{4}{D}\gamma_{SA} \tag{5}$$

and in a liquid is

$$\sigma_{SL} = E\varepsilon + \frac{4}{D}\gamma_{SL} \tag{6}$$

where γ_{SA} and γ_{SL} are interfacial surface tensions of the solid–air and solid–liquid interfaces, respectively. At a given strain, the difference between the stresses measured in air and liquid is

$$\Delta\sigma_f = \sigma_{SA} - \sigma_{SL} = \frac{4}{D}(\gamma_{SA} - \gamma_{SL}) \tag{7}$$

For a liquid in contact with a polymeric surface the Young/Dupre equation is

$$\gamma_{SA} - \gamma_{SL} = \gamma_{LA} \cos\theta \tag{8}$$

where θ is the contact angle. Upon substitution, equation (7) is given by

$$\Delta\sigma_f = \frac{4}{D}\gamma_{LA} \cos\theta \tag{9}$$

The morphology of Celgard 2400 (*Figure 1*) suggests a model of crystalline lamellae in series with parallel arrays of fibres is most representative. If the fraction of fibres in the cross-section is A_f and the average diameter is $\bar{D}$, the difference between the restoring force in air and a liquid of surface tension γ_{LA} is given by

$$\Delta\sigma = \frac{4A_f\gamma_{LA}\cos\theta}{\bar{D}} \tag{10}$$

Since $\Delta\sigma$ is the measured stress depression, the average fibre diameter can be calculated from equation (10).

Calculation of fibril diameter

The average fibril diameter at 10% strain was calculated from the data in *Figure 12* for those water/ethanol solutions which wet Celgard, that is which have a contact angle less than 90°. A fibre fraction A_f of 0.5 was used to obtain the results tabulated in *Table 2*. The average microfibril diameter is about 3.6 nm. This fibril diameter is much smaller than that observed by microscopic techniques[29], but at least two investigations have reported subfibrillation of craze material in polystyrene at this size scale[30,31].

In a given liquid where ($\gamma_{LA}\cos\theta$) is constant, equation (10) predicts that the fibre diameter is proportional to $A_F/\Delta\sigma$. With the assumption that A_F does not change during deformation, the stress depression in ethanol (*Figure 5*) was used to calculate the fibre diameter at various strains. The average microfibre diameter given in *Table 3* decreases by a factor of 4 from 2% to 10% strain consistent with a stress-induced subfibrillation mechanism. At higher strains the average microfibre diameter does not change. The assumption of constant A_F is not strictly valid since the void volume changes considerably during the initial 10% strain. Gradually decreasing A_F in the calculations would result in larger changes in $\bar{D}$ than indicated in *Table 3*.

Data from four different experiments are plotted as a function of the imposed stress in air in *Figure 14*. Stress depression values at various strains (*Figure 5*), stress depression values from the creep and stress relaxation experiments (*Figure 9*), and stress differences from stress–strain curves (*Figure 7*) are plotted on the ordinate. Only data in the region of subfibrillation, 0 to 10% strain, are included in the plot. Superposition of the data on a straight line which passes through the origin demonstrates that subfibrillation is controlled by the imposed external stress. The corresponding fibril diameters are included in the plot. Since $\Delta\sigma$ is inversely proportional to the fibril diameter, the stress required for subfibrillation increases continually as the fibril diameter decreases. It appears that the limit is on the order of 20 Å. The stress required to obtain this fibril size (50 MPa) is identical to the reported yield stress of the precursor material[29]. Consequently, as the imposed stress exceeds 50 MPa, deformation of the lamellae becomes predominant.

Table 3 Calculated average microfibre diameter in Celgard as a function of strain

Strain (%)	$\bar{D}$ (nm)
2	11.4
5	6.7
10	3.0
15	2.7
25	2.7
40	3.0
60	3.5

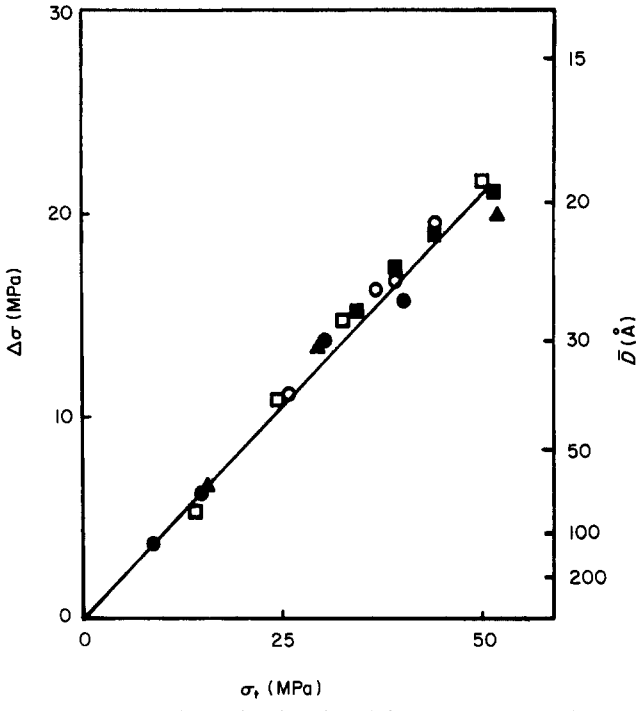

Figure 14 Stress depression in ethanol from 0 to 10% strain as a function of imposed stress

CONCLUSIONS

The phenomenon of stress depression observed when Celgard 2400 is exposed to certain liquids has been utilized to probe the role of surface stresses in hard elastic behaviour. The following conclusions can be made from this study:

(1) Surface stresses contribute 40% of the restoring force at strains up to 10%; above 10% strain there is no change in the magnitude of the surface contribution.

(2) Assuming that the surface stresses arise from fibrous entities observed in the electron microscope, a constitutive equation has been developed from which the fibril diameter can be calculated.

(3) Calculated values of the fibril diameter as a function of strain show that stress-induced subfibrillation is the mechanism responsible for the gradual increase in the surface stress up to 10% strain.

(4) Subfibrils are stable only under an imposed stress, the smallest fibril diameter obtained with this material is approximately 20 Å.

REFERENCES

1 Sprague, B. S. *J. Macromol. Sci.–Phys.* 1973, **B8**, 157
2 Knoblock, F. W. and Statton, W. O., US Pat. 3,299,171 (17 Jan. 1967) assigned to E. I. DuPont de Nemours and Company, Inc
3 Noether, H. D., US Pat. 3,313,110 (19 May 1970) assigned to Celanese Research Corporation
4 Quynn, R. G. and Sprague, B. S. *J. Polym. Sci. A-2*, 1970, **8**, 1971
5 Quynn, R. G., Brody, H., Sobering, S. E., Park, I. K., Foley, R. L., Noether, H. D., Whitnery, W., Pritchard, R., Sieminski, M. A., Hutchison, J. D., Wagner, H. L., Sakasku, J. K. and Corneliussen, R. *J. Macromol. Sci.–Phys.* 1970, **B4**, 953
6 Ishikawa, H., Numa, H. and Nagura, M. *Polymer* 1979, **20**, 516
7 Miles, M. J. and Baer, E. *J. Mater. Sci.* 1979, **14**, 1254
8 Moet, A., Palley, I. and Baer, E. *J. Appl. Phys.* 1980, **51**, 5175
9 Noether, H. D. and Whitney, W. *Colloid Polym. Sci.* 1973, **251**, 991
10 Clark, E. S. in 'Structure and Properties of Polymer Films', (Eds. R. W. Lenz and R. S. Stein), Plenum, New York, 1973
11 Park, I. K. and Noether, H. D. *Colloid Polym. Sci.* 1975, **253**, 824
12 Samuels, R. J. *J. Polym. Sci., Polym. Phys. Edn.* 1979, **17**, 535
13 Sarada, T. and Sawyer, L. C. *J. Membrane Sci.* 1983, **15**, 97
14 Miles, M., Petermann, J. and Gleiter, H. *J. Macromol. Sci.–Phys.* 1976, **12**, 523
15 Cackovic, H., Hosemann, R. and Loboda-Cackovic, J. *J. Polym. Sci., Polym. Lett. Edn.* 1978, **16**, 129
16 Wool, R. P., Lohse, M. I. and Rowland, T. J. *J. Polym. Sci., Polym. Lett. Edn.* 1979, **17**, 385
17 Wool, R. P. *J. Polym. Sci., Polym. Phys. Edn.* 1976, **14**, 603
18 Noether, H. D. and Brody, H. *Textile Res. J.* 1976, **46**, 467
19 Wool, R. P., paper No. 21S presented at the 69th Annual Meeting of AICHE, Chicago, 1976
20 Chen, Y. L., Ko, F. K. and Lundberg, J. L. *Polym. Eng. Sci.* 1976, **16**, 406
21 Cannon, S. L., McKenna, G. B. and Statton, W. O. *Macromol. Rev.* 1976, **11**, 209
22 Kambour, R. P. and Kopp, R. W. *J. Polym. Sci.* 1969, **7**, 183
23 Bucknall, C. B. *Br. Plast.* 1981, **40**, 84
24 Walton, K., Moet, A. and Baer, E., Contemporary Topics in Polym. Sci., Vol. 4, Plenum Publ. Corp., 1982
25 Walton, K., Moet, A. and Baer, E. 'The Interaction of Liquid Environment with Hard Elastic High Impact Polystyrene', in 'Structure–Property Relationships of Polymeric Solids', (Ed. A. Hiltner), Plenum, New York, 1983
26 Adamson, A. W. 'Physical Chemistry of Surface', Interscience Pub. Inc., New York, 1982
27 Graham, D. *J. Phys. Chem.* 1964, **68**, 2788
28 Van Krevelen, D. W. 'Properties of Polymers', Elsevier Publ. Co., New York, 1972, p. 166
29 Berenbaum, H. S., Isaacson, R. B., Druin, M. L. and Polvan, S. G. *Ind. Eng. Chem. Prod. Res. Dev.* 1974, **13**, 2
30 Beahan, P., Bevis, M. and Hull, D. *J. Mater. Sci.* 1972, **8**, 162
31 Brown, H. R. and Kramer, E. J. *J. Macromol. Sci.–Phys.* 1981, **19**, 487